JOURNAL OF COMPUTATIONAL PHYSICS **125,** 42–58 (1996)
ARTICLE NO. 0078

Capturing Shock Reflections: An Improved Flux Formula

ROSA DONAT AND ANTONIO MARQUINA*

Universitat de València 46100-Burjassot, València, Spain

Received January 3, 1995; revised July 12, 1995

Godunov type schemes, based on exact or approximate solutions to the Riemann problem, have proven to be an excellent tool to compute approximate solutions to hyperbolic systems of conservation laws. However, there are many instances in which a particular scheme produces inappropriate results. In this paper we consider several situations in which Roe's scheme gives incorrect results (or blows up all together) and we propose an alternative flux formula that produces numerical approximations in which the pathological behavior is either eliminated or reduced to computationally acceptable levels.

1. INTRODUCTION

Shock capturing techniques for the computation of discontinuous solutions to hyperbolic conservation laws are based on an old (by now) theorem of Lax and Wendroff establishing that the limit solutions of a consistent scheme in conservation form are in fact weak solutions to the PDE and, thus, their discontinuities will propagate at the right speeds.

Over the years, it has become clear that one of the most successful strategies for designing a shock-capturing scheme is to follow Godunov's lead and use the solution to the Riemann problem (the only initial-value problem easy enough to be solved explicitly) as an essential building block of the scheme.

Godunov assumed that a flow solution could be represented by a series of piecewise constant states with discontinuities at the cell interfaces. A piecewise constant function is a reasonable numerical representation of the solution in regions of smooth flow and it is especially well suited near discontinuities. The discretized flow solution is evolved by considering the nonlinear interaction between its component states. Viewed in isolation, each pair of neighboring states constitutes a Riemann problem, which can be solved exactly. If there is no interaction between neighboring Riemann problems, the global solution is easily found by piecing together these Riemann solutions. The approximate solution at the next time level is then obtained averaging over each cell this global solution.

The method can be written in conservation form since it uses solutions to Riemann problems which are themselves exact solutions of the conservation laws and, because it mimics much of the relevant physics, Godunov's scheme results in an accurate and well-behaved treatment of shock waves.

For gas dynamics simulations, Godunov's method computes the exact solution to a Riemann problem at each cell interface. However, most of the structure of the exact solution is lost in the averaging process used to update each cell value. This observation suggests that it may not be worthwhile calculating the Riemann solution exactly. In fact, one may be able to obtain equally good numerical results with an approximate Riemann solution obtained by some less expensive means.

Roe's scheme is based on a local linearization that makes the solution of the Riemann problem a trivial task. The solution to Roe's linearized Riemann problem coincides with the solution to the exact problem whenever this involves merely a single shock or contact discontinuity. On the other hand, since rarefaction waves do not appear in linear systems, the scheme can (and does) produce nonphysical expansion shocks in the computed flows.

Other approximate Riemann solvers, based on Roe's simplification, have emerged over the years. Their basic design principle is (as in Roe's scheme) that it might be sufficient to find only an approximate solution to a Riemann problem, provided that this approximate solution still describes important nonlinear behavior [9, 3].

Godunov type schemes are indeed very robust in most situations. However, they can, on occasions, fail quite spectacularly. For example, when computing shock reflection problems in one dimension, most shock capturing schemes produce an unphysical "overheating" near the reflecting wall [15]. In two dimensions, Roe's method can sometimes admit solutions with an inexplicably kinked Mach stem.

Reports on approximate Riemann solver failures and their respective corrections are abundant in the literature (see, e.g., [17] and references therein). It should be noted that the failures of a specific Riemann solver may usually

* E-mail: marquina@godella.matapl.uv.es; E-mail: donat@godella.matapl.uv.es. Supported by DGICYT PB94-0987, in part by a Grant from the I.V.E.I., in part by a Grant from Universitat de València and computer time supported in part by ARPA URI Grant ONR-N00014-92-J-1890.

0021-9991/96 $18.00

be repaired by the judicious use of a small amount of artificial dissipation. However, this technique often implies the tuning and re-tuning of various parameters, which degrades the automatic character of Godunov type schemes. Moreover, the type and amount of viscosity to be added in each particular deficiency is, usually, not the same, further aggravating the user.

A different strategy, described by Quirk [17], is to combine two or more solvers. With this approach, it is possible to control certain instabilities by changing the flavor of the dissipation mechanism rather than increasing the absolute level of dissipation.

Quirk's approach is very attractive, although it still has a user-problem dependent parameter left: when and where to use one Riemann solver in preference to another.

Our approach is similar to that of Quirk's. We do combine Roe's solver with a Lax–Friedrichs type of scheme to produce an entropy-satisfying, shock-capturing scheme, but the two solvers are intertwined in a more intrinsic way so that there are no adjustable parameters in the scheme.

In the present paper we address various instances in which there is a recognized failure of Roe's solver and propose an alternative flux formula that seems to alleviate or cure the problem.

The paper is organized as follows: In Section 2 we describe Marquina's flux formula for systems of hyperbolic conservation laws. In the scalar case, it corresponds to a flux formula used by Shu and Osher [22]. In Section 3 we apply it to Burgers' equation and compare the numerical results with those obtained with other well-known upwind flux formulae. Section 4 is devoted to the analysis of the overheating phenomenon that appears in shock reflection experiments and to several somewhat related questions. In Section 5, Marquina's scheme is used to approximate a slowly moving shock wave. We measure the level of noise generated by the scheme in the downstream region of the shock wave and compare it to that of Roe's scheme. Section 6 shows the performance of the proposed flux formula in 2D flows, analyzing the classical Mach 3 step flow. Some conclusions are drawn in Section 7.

2. ROE'S FLUX FORMULA, FLUX-SPLITTING SCHEMES AND AN ALTERNATIVE FLUX FORMULA

Disregarding entropy consideration, Roe's solver applied to a system of conservation laws in one dimension,

$$\mathbf{u}_t + (\mathbf{f}(\mathbf{u}))_x = 0, \tag{1}$$

yields a conservative method whose numerical flux function is computed as

$$\mathbf{F}^R(\mathbf{u}_l, \mathbf{u}_r) = \frac{1}{2}\left(\mathbf{f}(\mathbf{u}_l) + \mathbf{f}(\mathbf{u}_r) - \sum_p |\lambda_p|\alpha_p \mathbf{r}^p\right), \tag{2}$$

where

$$\alpha_p = \mathbf{l}^p \cdot (\mathbf{u}_l - \mathbf{u}_r)$$

and λ_p, $\mathbf{r}^p$, and $\mathbf{l}^p$ are the eigenvalues, (normalized) right and left eigenvectors, respectively, of $\tilde{A} = A(\tilde{\mathbf{u}}) = A(\mathbf{u}_l, \mathbf{u}_r)$, the Jacobian matrix $(\partial \mathbf{f}(\mathbf{u})/\partial \mathbf{u})$ at $\tilde{\mathbf{u}}$, the "Roe mean" of the left and right states (see, e.g., [10]).

The numerical flux formula of Roe's method (2) is in fact the flux at the origin corresponding to the Riemann problem for the constant coefficient system

$$\mathbf{u}_t + A(\mathbf{u}_l, \mathbf{u}_r)\mathbf{u}_x = 0 \tag{3}$$

with left and right states $\mathbf{u}_l$ and $\mathbf{u}_r$, respectively. Roe's definition of $A(\mathbf{u}_l, \mathbf{u}_r)$ guarantees (among other things) a Riemann solution that agrees with the exact Riemann solution to the original non-linear system in the special case, where $\mathbf{u}_l$ and $\mathbf{u}_r$ are connected by a single shock wave or a contact discontinuity.

However, Riemann solutions to linear systems such as (3) consist of only discontinuities, with no rarefaction waves. This can lead (and indeed it does) to numerical approximations with entropy violating discontinuities. To prevent these expansion shocks, the flux function in Roe's scheme needs to be modified. Harten and Hyman [7] introduce an intermediate state that simulates the diffusion introduced to a Godunov-type scheme by a continuous transition between the left and right states. Roe [20] describes another modification that breaks down expansion shocks and it also eliminates the "glitches" (dogleg phenomenon) that appear in most first-order schemes.

As usual, the one-dimensional scalar equation is a useful study case and it is particularly relevant to our discussion since it provides the starting point for Marquina's flux formula.

In [25], Van Leer considers the upwind-differencing first-order schemes of Godunov, Roe, and Engquist-Osher (E-O) for the inviscid Burgers equation. He observes that the difference between the E-O scheme and Godunov's method lies in the treatment of transonic shocks, while Roe and Godunov's schemes differ only at transonic expansions, where the exact Riemann solver, used in Godunov's method, would include an expansion fan, Roe's method puts in a so-called expansion shock, i.e., an entropy violating discontinuity. An entropy fix is necessary to obtain physically relevant numerical approximations with Roe's method in these situations.

In the scalar case, Marquina's flux formula is a combination of Roe's flux and a local Lax–Friedrichs (LLF from now on) flux utilized by Shu and Osher in [22] and labeled F^{RF}:

$$F^{\mathrm{RF}}(u_l, u_r) = \begin{cases} f(u_l) & \text{if } f' > 0 \text{ in } [u_l, u_r] \\ f(u_r) & \text{if } f' < 0 \text{ in } [u_l, u_r] \\ \frac{1}{2}\left(f(u_l) + f(u_r) - \alpha(u_r - u_l)\right) & \text{else} \end{cases} \tag{4}$$

$$\alpha = \max_{u \in [u_l, u_r]} |f'(u)|. \tag{5}$$

Throughout this section, $[u_l, u_r]$ should be understood as the range of u-values that lie between u_l and u_r.

Formula (4) is equivalent to Godunov's flux formula (see, e.g., [12])

$$F^{\mathrm{G}}(u_l, u_r) = \begin{cases} \min_{u_l \le u \le u_r} f(u) & \text{if } u_l \le u_r \\ \max_{u_r \le u \le u_l} f(u) & \text{if } u_l > u_r \end{cases} \tag{6}$$

whenever f' does not change sign between the left and right states. If this is not the case, F^{RF} is obtained by switching to the more viscous, entropy satisfying Lax–Friedrichs scheme. It can be verified (see [22]) that the LLF flux

$$F^{\mathrm{LLF}}(u_l, u_r) = \tfrac{1}{2}\left(f(u_l) + f(u_r) - \alpha(u_r - u_l)\right)$$

is monotone; hence F^{RF} is an "entropy fix" for Roe's flux.

The experiments reported in [22] and our own experimentation confirms that conservative schemes whose numerical flux function is F^{RF} always approximate the physically relevant solution even for non-convex f. Moreover, local pathologies, like the dogleg effect, either do not show up in numerical approximations, or are reduced to $O(\Delta x)$ glitches in the first order version of the scheme. Higher order versions completely eliminate the pathology.

In the convex case, the schemes of Roe and Godunov differ only at transonic rarefactions; in this case we would only need to switch to LLF when $f'(u_l) < 0 < f'(u_r)$ but we keep (4) as established because it is more general and it works properly also for non-convex conservation laws.

The extension to systems of conservation laws differs from that of [22] and follows two basic directions. On one hand, Roe's linearization (or any linearization, as pointed out in [4]) may not always be appropriate, especially when dealing with systems of conservation laws other than the Euler equations for which the "Roe mean" might not be easily computed (or even known). Along this line, and still in the upstream-differencing spirit, we shall make use of two sets of eigenvalues and eigenvectors, one coming from the left state and the other coming from the right state, to compute the flux at a given interface.

On the other hand, the combination of Roe's solver with the LLF scheme is done *locally*. The choice of scheme is done in each "local" characteristic field, thus the scheme for systems of conservation laws mimics the properties of the scheme for the scalar conservation law.

The algorithmic description of Marquina's flux formula is as follows:

Given the left and right states, we compute the "*sided*" local characteristic variables and fluxes:

$$\omega_l^p = \mathbf{l}^p(\mathbf{u}_l) \cdot \mathbf{u}_l \quad \phi_l^p = \mathbf{l}^p(\mathbf{u}_l) \cdot \mathbf{f}(\mathbf{u}_l)$$
$$\omega_r^p = \mathbf{l}^p(\mathbf{u}_r) \cdot \mathbf{u}_r \quad \phi_r^p = \mathbf{l}^p(\mathbf{u}_r) \cdot \mathbf{f}(\mathbf{u}_r)$$

for $p = 1, 2, ..., m$. Here $\mathbf{l}^p(\mathbf{u}_l)$, $\mathbf{l}^p(\mathbf{u}_r)$, are the (normalized) left eigenvectors of the Jacobian matrices $A(\mathbf{u}_l)$, $A(\mathbf{u}_r)$.

Let $\lambda_1(\mathbf{u}_l), ..., \lambda_m(\mathbf{u}_l)$ and $\lambda_1(\mathbf{u}_r), ..., \lambda_m(\mathbf{u}_r)$ be their corresponding eigenvalues. We proceed as follows:

For $k = 1, ..., m$,

If $\lambda_k(\mathbf{u})$ does not change sign in $[\mathbf{u}_l, \mathbf{u}_r]$, then

```
If λ_k(u_l) > 0 then
    φ_+^k = φ_l^k
    φ_-^k = 0
else
    φ_+^k = 0
    φ_-^k = φ_r^k
endif
```

else

$$\alpha^k = \max_{\mathbf{u} \in \Gamma(\mathbf{u}_l, \mathbf{u}_r)} |\lambda_k(\mathbf{u})|$$
$$\phi_+^k = 0.5(\phi_l^k + \alpha_k \omega_l^k)$$
$$\phi_-^k = 0.5(\phi_r^k - \alpha_k \omega_r^k)$$

endif

$\Gamma(\mathbf{u}_l, \mathbf{u}_r)$ is a curve in phase space connecting $\mathbf{u}_l$ and $\mathbf{u}_r$. For the Euler equations of gas dynamics, the fields are either genuinely non-linear or linearly degenerate; hence we can test the possible sign changes of $\lambda_k(\mathbf{u})$ by checking the sign of $\lambda_k(\mathbf{u}_l) \cdot \lambda_k(\mathbf{u}_r)$. Also, α_k can be determined as

$$\alpha_k = \max\{|\lambda_k(\mathbf{u}_l)|, |\lambda_k(\mathbf{u}_r)|\}.$$

Marquina's flux formula is then

$$\mathbf{F}^{\mathrm{M}}(\mathbf{u}_l, \mathbf{u}_r) = \sum_{p=1}^{m} \left(\phi_+^p \mathbf{r}^p(\mathbf{u}_l) + \phi_-^p \mathbf{r}^p(\mathbf{u}_r)\right), \tag{7}$$

where $\mathbf{r}^p(\mathbf{u}_l)$, $\mathbf{r}^p(\mathbf{u}_r)$ are the right (normalized) eigenvectors of the Jacobian matrices $A(\mathbf{u}_l)$, $A(\mathbf{u}_r)$.

Marquina's numerical flux is consistent, i.e.,

$$\mathbf{F}^{\mathrm{M}}(\mathbf{u}, \mathbf{u}) = \mathbf{f}(\mathbf{u}),$$

and, in fact, when applied to a constant coefficient one-dimensional system, Marquina's scheme is equivalent to

Roe's and would yield the exact solution to the Riemann problem.

Notice also that when all signal speeds associated to the numerical flux $\mathbf{F}^{\mathrm{M}}(\mathbf{u}, \mathbf{v})$ are >0 then

$$\mathbf{F}^{\mathrm{M}}(\mathbf{u}, \mathbf{v}) = \mathbf{f}(\mathbf{u})$$

and when all signal speeds are <0,

$$\mathbf{F}^{\mathrm{M}}(\mathbf{u}, \mathbf{v}) = \mathbf{f}(\mathbf{v}).$$

Marquina's numerical flux (7) has a clear flux-splitting structure, with

$$\mathbf{F}^{\mathrm{M}}(\mathbf{u}, \mathbf{v}) = \mathbf{F}^{+} + \mathbf{F}^{-},$$

where

$$\mathbf{F}^{+} = \sum \phi_{+}^{p}(\mathbf{u}, \mathbf{v})\mathbf{r}^{p}(\mathbf{u}), \quad \mathbf{F}^{-} = \sum \phi_{-}^{p}(\mathbf{u}, \mathbf{v})\mathbf{r}^{p}(\mathbf{u}) \tag{8}$$

but notice that, here, the characteristic numerical fluxes $\phi_{\pm} = \phi_{\pm}(\mathbf{u}, \mathbf{v})$ depend (in a non-linear way) on the left and right states.

For non-linear systems in which the flux function is homogeneous of degree one, such as the gas dynamics equations for an ideal gas, Marquina's formula reduces to the Steger–Warming flux vector split formula when there is no change in sign in any of the eigenvalues.

Indeed, if $\mathbf{f}(\mathbf{u}) = A(\mathbf{u}) \cdot \mathbf{u}$ then

$$\phi_{l}^{p} = \mathbf{l}^{p}(\mathbf{u}_{l}) \cdot \mathbf{f}(\mathbf{u}_{l}) = \lambda_{p}(\mathbf{u}_{l})\, \omega_{l}^{p}$$
$$\phi_{r}^{p} = \mathbf{l}^{p}(\mathbf{u}_{r}) \cdot \mathbf{f}(\mathbf{u}_{r}) = \lambda_{p}(\mathbf{u}_{r})\, \omega_{r}^{p};$$

thus, when $\lambda_{p}(\mathbf{u}_{l}) \cdot \lambda_{p}(\mathbf{u}_{r}) \geq 0$, $p = 1 \cdots m$,

$$\phi_{+}^{p} = \max(\lambda_{p}(\mathbf{u}_{l}), 0) \cdot \omega_{l}^{p} = \lambda_{p}^{+}(\mathbf{u}_{l}) \cdot \omega_{l}^{p}$$
$$\phi_{-}^{p} = \min(\lambda_{p}(\mathbf{u}_{r}), 0) \cdot \omega_{r}^{p} = \lambda_{p}^{-}(\mathbf{u}_{r}) \cdot \omega_{r}^{p}$$

and

$$\mathbf{F}^{+} = \sum \phi_{+}^{p}\mathbf{r}^{p}(\mathbf{u}_{l}) = \sum \lambda_{p}^{+}(\mathbf{u}_{l})\omega_{l}^{p} \cdot \mathbf{r}^{p}(\mathbf{u}_{l}) = A^{+}(\mathbf{u}_{l}) \cdot \mathbf{u}_{l}$$
$$\mathbf{F}^{-} = \sum \phi_{-}^{p}\mathbf{r}^{p}(\mathbf{u}_{r}) = \sum \lambda_{p}^{-}(\mathbf{u}_{r})\omega_{r}^{p} \cdot \mathbf{r}^{p}(\mathbf{u}_{r}) = A^{-}(\mathbf{u}_{r}) \cdot \mathbf{u}_{r}$$

with $A^{+}$and A^{-} defined as usual (see, e.g., [23]).

When the eigenvalue corresponding to a characteristic field changes sign across a given interface, $\mathbf{F}^{+}$ and $\mathbf{F}^{-}$ in (8) will depend on both the left and right states and these two flux formulae take different values.

For the equations of ideal gas dynamics Marquina's flux formula and Steger–Warming flux vector split formula yield, thus, similar results in most situations. However, we remark that (7) is more general: It can be applied to non-homogeneous fluxes, such as the flux in Burgers equation or the equations of gas dynamics for real gases [6].

The first-order scheme based on Marquina's flux formula is, thus,

$$\mathbf{u}_{j}^{n+1} = \mathbf{u}_{j}^{n} + \frac{\Delta x}{\Delta t}\left(\mathbf{F}^{\mathrm{M}}(\mathbf{u}_{j}^{n}, \mathbf{u}_{j+1}^{n}) - \mathbf{F}^{\mathrm{M}}(\mathbf{u}_{j-1}^{n}, \mathbf{u}_{j}^{n})\right).$$

Higher accuracy is obtained by a non-linear interpolation procedure of either the fluxes [22] or the dependent variables [10, 1] and a Runge–Kutta time-stepping procedure [22].

There are a variety of reconstruction procedures available to increase the formal order of spatial accuracy of the method. In our experiments, we have chosen the ENO (essentially non-oscillatory) polynomials of Harten *et al.* [10], Van Leer's piecewise linear reconstruction [24], and Marquina's piecewise hyperbolic method (PHM) [13].

ENO techniques (including the PHM) use a local adaptive stencil to obtain information automatically from regions of smoothness when the solution develops discontinuities. As a result, approximations using these methods can obtain uniformly high-order accuracy right up to the discontinuities, while keeping a sharp, essentially non-oscillatory shock transition (see [13, 10] and references therein).

If $\mathbf{R}(\cdot, \mathbf{u}^{n})$ is a reconstruction procedure that computes an $O(h^{p})$ approximation to $\mathbf{u}(x, t_{n})$ from the cell values $\{\mathbf{u}^{n}\}$, then the pth-order version of the scheme based on such a reconstruction procedure is obtained following a semi-discrete formulation, i.e.,

$$\frac{d}{dt}\mathbf{u}_{j}(t) = \frac{1}{\Delta x}[\tilde{\mathbf{f}}_{j+1/2} - \tilde{\mathbf{f}}_{j-1/2}], \tag{9}$$

where

$$\tilde{\mathbf{f}}_{j+1/2} = \mathbf{F}(\mathbf{R}(x_{j+1/2} - 0; \mathbf{u}(t)), \mathbf{R}(x_{j+1/2} + 0; \mathbf{u}(t)))$$

and $\mathbf{F}(\mathbf{u}_{1}, \mathbf{u}_{2})$ is the exact or approximate Riemann solver flux to be used.

Considering (9) to be a system of ordinary differential equations in t for the vector $\mathbf{u}(t) = \{\mathbf{u}_{j}(t)\}$, we solve the problem using a numerical ODE solver. In particular, in our experiments we use Shu and Osher [22] TVD Runge–Kutta solvers of second and third order.

We recall (see [10, 13]) that these scalar reconstructions are non-oscillatory only if the discontinuities are separated by at least $r + 1$ points of smoothness, where r is the order of accuracy of the reconstruction. Consequently, a component-by-component reconstruction procedure may cease to be non-oscillatory around the discrete set of points

where discontinuities of the solution interact and can produce "noise" around this set of points. One can largely avoid the noise derived from this fact by applying the reconstruction procedure to the "local characteristic variables" (see [10]).

In [22], Shu and Osher use the moving-stencil idea directly on numerical fluxes to get ENO schemes without using cell-averages. For systems, the reconstruction procedure is applied in each "local characteristic field," and the starting point in the choice of stencil process has to be done in an "upwind" way. We refer to [22] for further details.

We have implemented the higher order versions of the method following both approaches obtaining very similar results.

3. THE SCALAR CONSERVATION LAW

In this section we discuss the differences between the Shu–Osher F^{RF} flux formula (4), i.e., Marquina's flux formula for scalar equations and other well-known upwind schemes on the basis of the inviscid Burgers equation.

We shall consider the schemes of Roe, with Harten–Hyman entropy fix [7] (R-H), Engquist-Osher (E-O), and a flux-splitting scheme (labeled S-W).

For Burgers equation, the fluxes corresponding to the R-H and E-O methods can be expressed as follows (see, e.g., [12, 25]):

$$F^{\mathrm{RH}}(u_l, u_r) = \begin{cases} 0.5u_l^2 + \dfrac{u_r - \hat{a}}{u_r - u_l}(u_r - u_l) & \text{if } u_l < 0 < u_r \\ 0.5u_r^2 & \text{if } \hat{a} < 0 \\ 0.5u_l^2 & \text{if } \hat{a} > 0 \end{cases} \tag{10}$$

$$\hat{a} = \tfrac{1}{2}(u_r + u_l) \tag{11}$$

$$F^{\mathrm{EO}}(u_l, u_r) = \tfrac{1}{2}\{(u_l^+)^2 + (u_r^-)^2\}. \tag{12}$$

We shall consider also a naïve extension (or rather, a "restriction") of Steger and Warming flux-vector split formula [23] to Burgers equation, for which $f(u) = 1/2 f_u u \neq f_u u$. This flux vector is not a homogeneous function and the analysis in [23] does not follow through. However, the flux formula

$$\begin{aligned} F^{\mathrm{SW}}(u_l, u_r) = \tfrac{1}{2}\,&(f(u_l) + f(u_r) \\ &- (|f'(u_r)| \cdot u_r - |f'(u_l)| \cdot u_l)) \end{aligned} \tag{13}$$

corresponds to the following splitting for the flux $f(u)$

$$\begin{aligned} f(u) &= f^+(u) + f^-(u) \\ f^+(u) &= \tfrac{1}{2}\{f(u) + |f_u| u\} \\ f^-(u) &= \tfrac{1}{2}\{f(u) - |f_u| u\}. \end{aligned}$$

For Burgers equation $f_u = u$ and it is easy to check that $(f^+)' \geq 0$ and $(f^-)' \leq 0$. Equation (13) provides, thus, a flux-splitting scheme for Burgers equation with the usual definitions.

To begin, let us consider the following IVP:

$$\begin{aligned} &u_t + \left(\frac{u^2}{2}\right)_x = 0 \\ &u(x, 0) = \begin{cases} -1 & \text{if } x < -0.5 \\ 1 & \text{if } -0.5 < x < 0.5 \\ -1 & \text{if } x > 0.5. \end{cases} \end{aligned} \tag{14}$$

Its solution consists of a centered rarefaction wave that contains a sonic point at $x = -0.5$ and a stationary shock wave located at $x = 0.5$. Figure 1 shows the approximate solutions obtained with each scheme.

Since $f(-1) = f(1)$, Roe's scheme without an entropy fix would substitute the rarefaction wave by an unphysical stationary expansion shock. As observed in Fig. 1, both entropy corrections to Roe's scheme (F^{RH} and F^{RF}) give absolutely similar computational results in the rarefaction area.

We observe an $O(\Delta x)$ glitch at the sonic point. This is to be expected, since only the sonic flux (the flux at the interface across which the characteristic speed changes sign) is modified (see Roe [20]). Notice that the dogleg effect at the sonic point is more acute in the E-O and flux-splitting schemes.

As noticed in [25], since the shock at $x = 0.5$ stands exactly on a cell boundary, the numerical solution obtained with Roe's method gives a shock profile with no interior points, while the E-O scheme produces two interior values. Marquina's scheme behaves here like the E-O scheme, while the flux-splitting scheme leads to a shock profile smeared over twice as many computational cells.

This example exhibits the behavior of Marquina's scheme as compared with the other three. Transonic rarefaction profiles are completely similar to those obtained with Roe's entropy-fixed scheme while transonic shock profiles are similar to those obtained with the E-O scheme. For non-transonic shock profiles, as well as non-transonic rarefactions, the numerical solutions obtained with these three schemes are similar, as observed in Fig. 2. The flux-splitting scheme produces shock profiles with a larger degree of smearing in all cases and poorer overall resolution. Here, the solution at $t = 0$ is as in (14) but with $u(x, 0) = 0.1$ for $x < 0.5$, $x > 0.5$. Thus, neither the shock nor the rarefaction wave cross the sonic point.

4. SHOCK REFLECTIONS, OVERHEATING, AND RELATED MATTERS

We study now the problem of a strong shock reflecting from a rigid wall. Conventional schemes applied to this

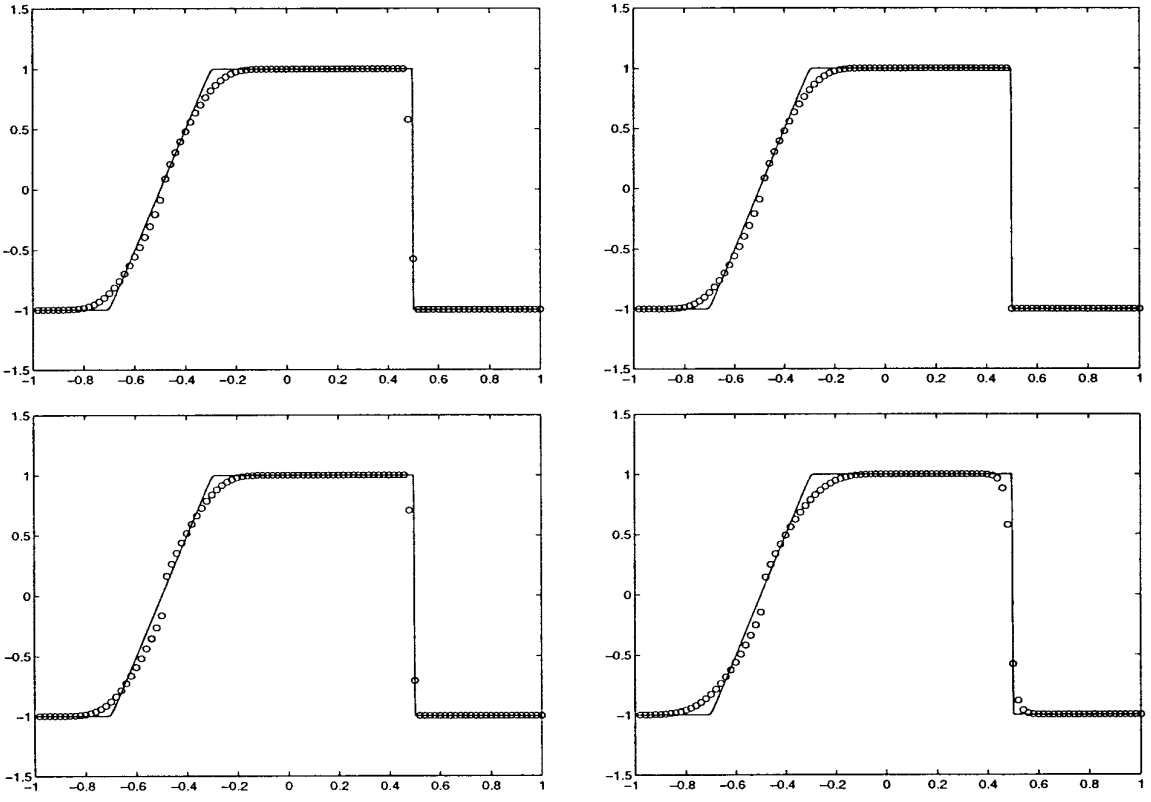

FIG. 1. First-order numerical approximations to a solution of Burgers equation containing a transonic shock and a transonic rarefaction. The solid line is the true solution. Marquina (top left); R-H (top right); E-O (bottom left); S-W (bottom right).

problem give numerical approximations with a consistent $O(1)$ error in the density and internal energy next to the wall.

Noh [15] investigated the ''excess heating error'' in the context of the artificial viscosity approach. Noh defines this error as the excess wall (or piston) heating, due to the artificial viscosity terms which occurs on shock formation (e.g., at a rigid wall where a gas is brought to rest and a shock propagated away, or at the sudden start up of a piston).

This type of error occurs in the first few zones near the wall and shows up as a peak in the specific internal energy (overheating) or, equivalently, a dip in the density. His analysis and experimentation leads him to conclude that the error is inevitable because it is built into the exact solution to the differential equations defining the artificial viscosity method. In fact he goes one step further and argues that such an error will necessarily occur for any shock-smearing method (in the absence of heat conduction) whether the viscosity occurs explicitly in the method or not.

In real fluids, heat conduction is present and this excess wall heating would not occur (since any hot spot would be quickly dissipated). Thus, Noh concludes that any method which introduces a heat conducting mechanism will, in principle, be able to reduce or even eliminate the overheating. Noh gives one such method in the artificial viscosity context.

Similar conclusions are attained by Menikoff in [14], where a detailed analysis of the wall heating error (again for artificial viscosity methods in Lagrangian and Eulerian formulations) is performed. Menikoff's argues that the numerical error is due to the artificial shock width and it mimics a real physical effect that has been observed in physical shock tubes. His line of reasoning leads him to conjecture that all shock capturing schemes without significant heat conduction will have the same type of qualitative entropy error.

Problems of this type have also been investigated by Glaister for more general equations of state [6]. The same phenomenon can be observed in his experiments.

Let us consider the one-dimensional Euler equations of gas dynamics for a polytropic gas, i.e., (1) with

$$\mathbf{u} = (\rho, M, E)^{\mathrm{T}}, \quad \mathbf{f}(\mathbf{u}) = q\mathbf{u} + (0, P, qP) \tag{15}$$

where ρ, q, M, E, and P are the density, velocity, moment,

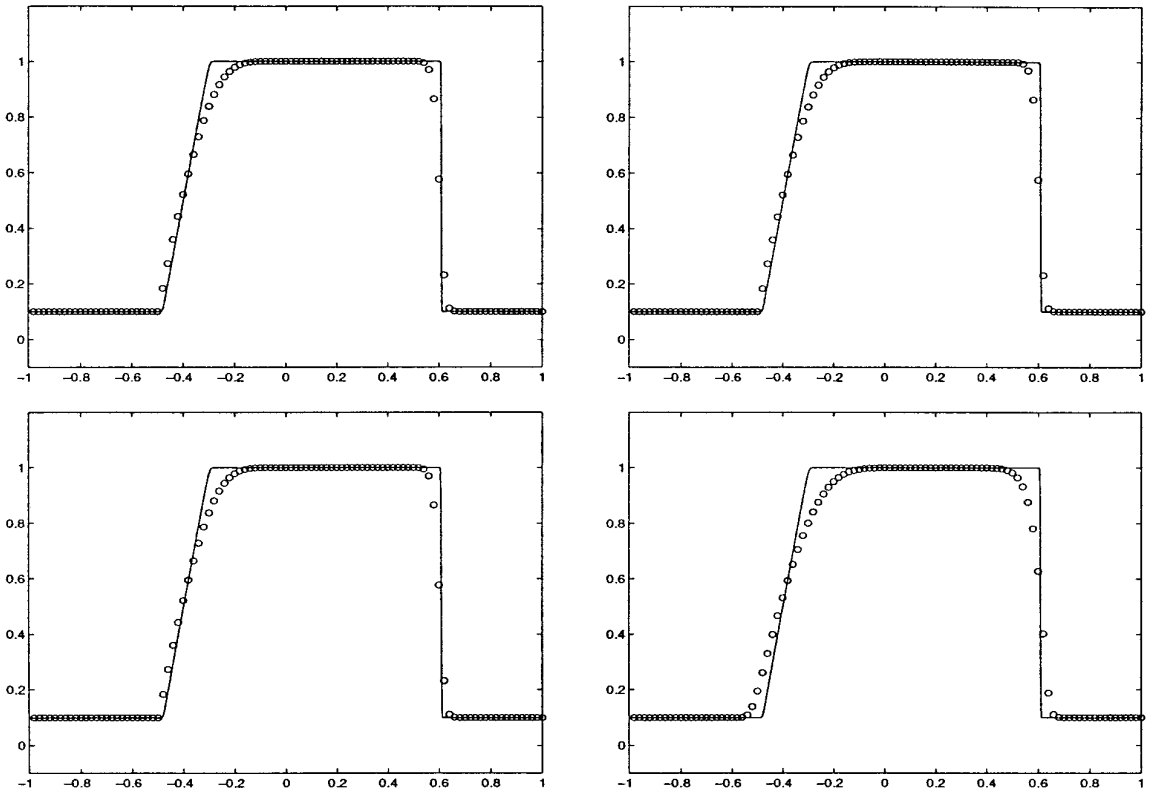

FIG. 2. First-order numerical approximations to a solution of Burgers equation containing non-transonic shock and rarefaction waves. The solid line is the true solution. Marquina (top left); R-H (top right); E-O (bottom left); S-W (bottom right).

energy, and pressure, respectively, with the following initial conditions at $t = 0$:

$$(\rho(x), q(x), P(x)) = (\rho_0, q_0, P_0), \quad 0 < x < 1. \tag{16}$$

This represents a gas of constant density and pressure moving towards $x = 1$ (provided $q_0 > 0$). The boundary at $x = 1$ is a rigid wall and the exact solution describes the shock reflection from the wall. The gas is brought to rest at $x = 1$ and, denoting the preshock values by $(-)$ and the postshock values by $(+)$ we can postulate an exact solution of the form

$$\rho = \rho^+, \quad q = q^+ = 0, \quad P = P^+ \qquad \text{for } (x-1)/t > S,$$
$$\rho = \rho^- = \rho_0, \quad q = q^- = q_0, \quad P = P^- = P_0 \quad \text{for } (x-1)/t < S,$$

where S, the speed at which the shock moves out of the wall and into the computational domain, is given by the Rankine–Hugoniot jump relations, i.e.,

$$S = \frac{[\rho u]}{[\rho]} = \frac{[P + \rho u^2]}{[\rho u]} = \frac{[u(e+P)]}{[e]}.$$

In our numerical experiments we take

$$P_0 = 10^{-3}; \quad \rho_0 = 1; \quad q_0 = 1$$

and the ideal gas equation of state with $\gamma = \frac{5}{3}$.

Figure 3 displays numerical approximations obtained with the first-order schemes of Marquina and Roe. It is worth noticing that the error at the bottom of the spike in the numerical approximation obtained with Marquina's solver is less than 1%. This should be compared with the 10% error at the bottom of the spike obtained with Roe's scheme (or even with the 100% error obtained with the standard artificial viscosity method [15]).

The second- and third-order extensions of Marquina's flux formula lead to numerical solutions in which the pathological behavior at the wall is consistent with that of the first-order scheme. On the contrary, the higher order extensions of Roe's scheme produce also a spurious overshoot before the final dip at the wall. Figure 4 shows a closeup look at the wall. We observe, on the same scale, the difference in magnitude between the overheating obtained with Roe's scheme and its higher order versions and Marquina's scheme and its corresponding higher order extensions. Notice that the numerical approximation obtained with Marquina's flux formula and the PHM provides the best resolution.

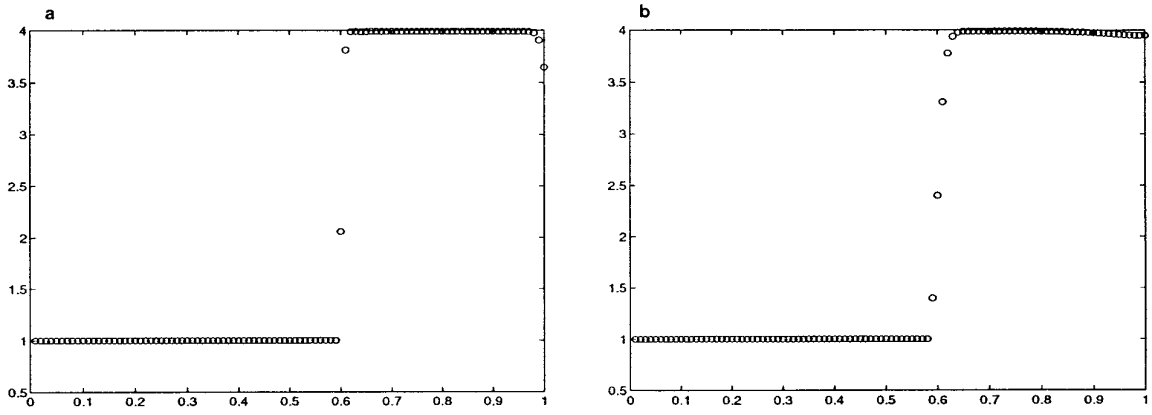

FIG. 3. First-order density profiles for the shock reflection problem: Roe left, Marquina right.

We can observe in Fig. 3 that the shock resolution in Marquina's first-order method is worse than in Roe's method. This is due to our implementation of Roe's scheme which does not incorporate an entropy fix (not necessary in this case since the analytical solution does not contain rarefaction waves). The reflecting boundary conditions imposed at the wall imply a sign change in the eigenvalue corresponding to the linearly degenerate field, which makes Marquina's scheme switch to the LLF flux formula. This leads to the observed shock transition. In general Roe's method needs to incorporate an entropy correction which would be turned on by the reflecting boundary conditions at the wall and would also incorporate viscosity to the shock, leading to a shock transition region similar to that obtained with Marquina's scheme. In any case the third-order versions of both methods only have two points in the shock transition region.

Our experiments show a very mild dependency of the magnitude of the error with respect to the Courant number. The numerical approximations shown in Figs. 3 and 4 have been obtained with $\Delta t/\Delta x = 0.2$. We ran the test for values of $\Delta t/\Delta x$ ranging between 0.1 to 0.6 which correspond to Courant numbers between 0.15 and 0.75. We have found that the value of the numerical solution at the wall is slightly larger when the Courant number increases, but the numerical values at the wall differ only about 0.2% at times for which the shock has left the wall completely. When the shock is formed, in the first steps of the computation, larger Courant numbers can lead to an increase of up to 2% in the numerical solution at the wall.

The overheating error decreases with time and the dependence of its magnitude with time is also quite mild. For example, for the first-order method the absolute value of the difference between the computed values with $\Delta t/\Delta x = 0.4$ at times $t = 0.8$ and $t = 1.6$ is about 0.015, which represents a 0.4% variation in the value of the numerical solution at the wall.

In the first few steps, Roe's scheme estimates erroneously the shock speed, which is essentially wrong by $O(1)$, this in turn gives $O(1)$ errors for the density. Roe's scheme

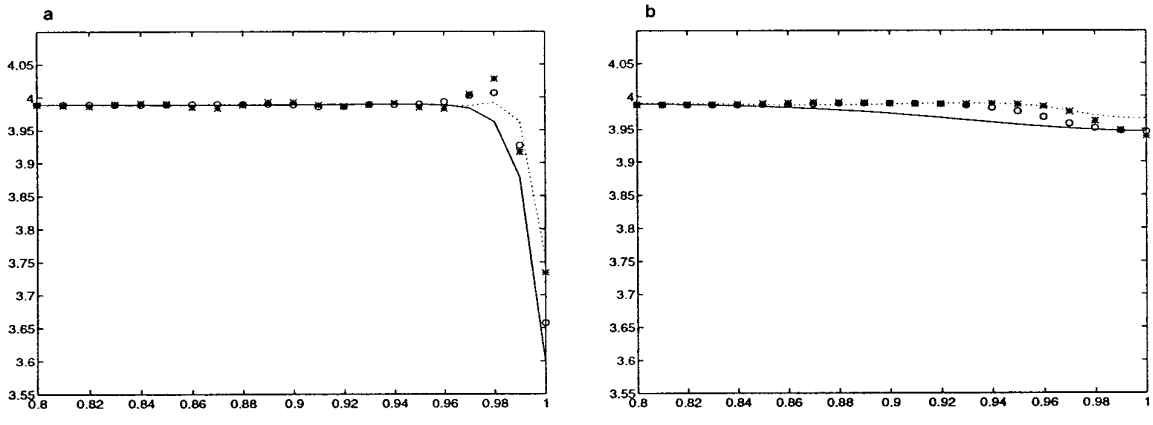

FIG. 4. A closer look to the overheating phenomenon: —— plain, ○ ENO2, * ENO3, ···, PHM.

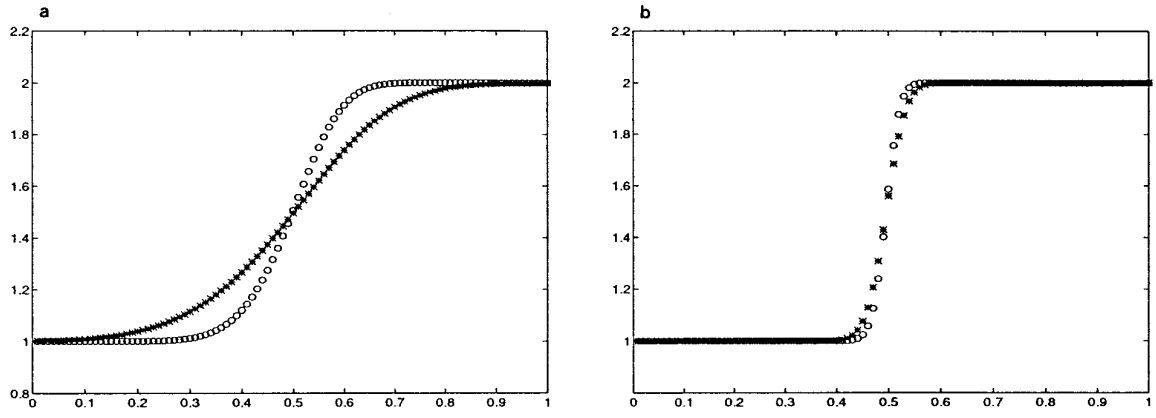

FIG. 5. Density smoothing due to the artificial heat conduction mechanism in Marquina's scheme: ○, $t = 1$, *, $t = 4$. First-order left, third-order right.

never recovers from these first steps errors because the error appears in the contact wave but, since the flow velocity is everywhere zero behind the shock wave, no dissipation is added via the contact wave to damp out the local error at the wall.

Marquina's scheme introduces an effective coupling between the equations (via the α) that acts as a dissipative mechanism, reducing the length of the spike to computationally acceptable levels.

Based on Noh's observations, we could interpret the behavior of the numerical solution obtained with Marquina's flux formula by saying that there may be an artificial heat conduction mechanism built into Marquina's solver which is responsible for the curbing of the spike.

It is well known (e.g., [9]) that flux-splitting schemes cannot exactly resolve stationary discontinuities. Contact discontinuities keep on spreading with the use of any split flux scheme.

It seems clear that Marquina's scheme does have a built-in heat conduction mechanism. To test the influence the flux formula has on stationary discontinuities we consider the Riemann problem with left and right states given by

$$(\rho_l = 1, q_l = 0, p_l = 1) \quad (\rho_r = 2, q_r = 0, p_r = 1) \tag{17}$$

whose solution is just a stationary (contact) discontinuity. Of course, Roe's scheme resolves perfectly this discontinuity (by design). Marquina's flux formula gives non-zero values when the velocity vanishes and the left and right pressures are equal. The artificial heat conduction mechanism tends to smooth out the density.

The result of Marquina's first-order accurate scheme is shown in Fig. 5. As we can see, the density is smoothed with the number of time steps, a property which is shared by most flux-vector-splitting schemes. In fact, the Steger–Warming flux formula leads to numerical results for the two experiments considered so far that are virtually indistinguishable from those produced by Marquina's flux formula (Marquina's scheme reduces to Steger–Warming's for the initial data considered in Fig. 5). This is an undesirable property when solving the Navier–Stokes equations in a boundary layer, and one should be careful in using the scheme in that situation. However, since the smoothing is less severe when we increase the order of the scheme, its higher order versions might still be suitable.

Roe's solver not only presents a local spike in the shock reflection case, this behavior can also be observed when an initial discontinuity breaks into two rarefaction waves moving in opposite directions, although in this case the use of any linearization (such as Roe's) might lead to the blow up of the scheme.

Einfeldt *et al.* show in [4] that certain choices of initial data will inevitably give rise to instabilities with any attempt to substitute linearized solutions because for these data, any linearization will yield a negative density or pressure. They express this fact by saying that certain Riemann problems are not linearizable.

Following [4] we consider the following class of initial data:

$$(\rho(x), q(x), P(x)) = \begin{cases} (\rho_0, q_0, P_0), & \text{if } x < 0.5; \\ (\rho_0, -q_0, P_0), & \text{if } x \geq 0.5. \end{cases} \tag{18}$$

If $q_0 > 0$, two shock waves are formed from the original jump in velocity. They propagate from the center of the interval with constant velocities in opposite directions and the gas remains at rest in between. This is a linearizable problem computationally equivalent to the shock reflection test problem already analyzed.

Numerically, we observe the same type of behavior for both schemes (Roe and Marquina's) as in the previous test (see Fig. 6). In our numerical experiments we have chosen $(\rho_0, q_0, P_0) = (1, 4, 1)$ and $\Delta t/\Delta x = 0.1$.

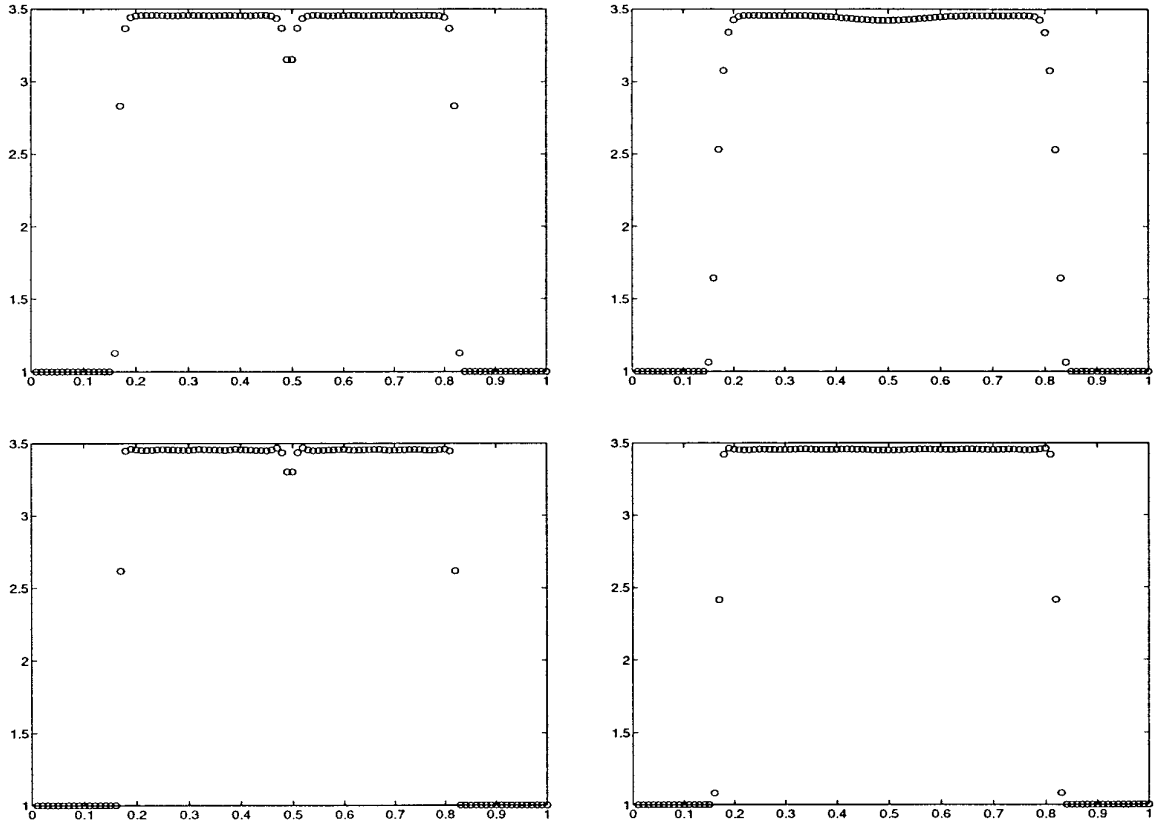

FIG. 6. Collision of two shocks of equal strength. First-order (top) and third-order (PHM, bottom) density profiles: Roe left, Marquina right.

As before, the error at the bottom of the spike in Marquina's solver is less than 1%, while the third-order (PHM) scheme has only a 0.3% error there. In this case, the hyperbolic reconstruction gives the best results, probably due to its more local character. ENO reconstructions (not shown) give slight oscillations of the order of the local truncation error.

If $q < 0$, the problem might not be linearizable, even though it has a solution with positive density and internal energy. The reason for the failure of the linearization is the occurrence of two rarefaction waves in the exact solution to the Riemann problem. Einfeldt *et al.* consider the particular case where $\rho_0 = 1$, $q_0 = -2$, $e_0 = 3$. This Riemann problem is not linearizable and Roe's scheme blows up after a few steps (but Roe's scheme with Harten's entropy fix does not; see [4]). Marquina's scheme behaves like the HLLE scheme described by Einfeldt [3, 4] (see Fig. 7).

Figure 7 displays the numerical approximation obtained with an ENO linear reconstruction. This particular reconstruction is also TVD (see [10] and references therein), a property which is not shared by higher order ENO reconstructions or Marquina's PHM. For this experiment, our third-order methods have failed, probably due to the almost vacuum conditions of the solution near $x = 0.5$.

On the other hand, taking $\rho_0 = 1$, $q_0 = -1$, $e_0 = 5$ as initial data leads to a linearizable problem for which the density exhibits non-smooth behavior similar to the shock reflection problem. As observed, the problem is alleviated by using Marquina's solver. Although the behavior of the numerical approximations obtained with the higher order extensions of Marquina's scheme is not as good as in the shock collision case, the density profiles are still smoother than those obtained with Roe's scheme (see Fig. 8).

5. SLOWLY MOVING SHOCKS

Another generic "deficiency" of most Godunov-type schemes, is the generation of numerical errors which occurs behind a nearly stationary shock. The phenomenon is inherent to nonlinear systems of equations (solutions of scalar conservation laws are perfectly well behaved) and typically shows up as a long wavelength noise in the downstream running wave family that is not effectively damped by the dissipation of the scheme.

Woodward and Colella [1, 28] were among the first to point out this deficiency for the first-order method of Godunov and MUSCL, one of its second-order extensions.

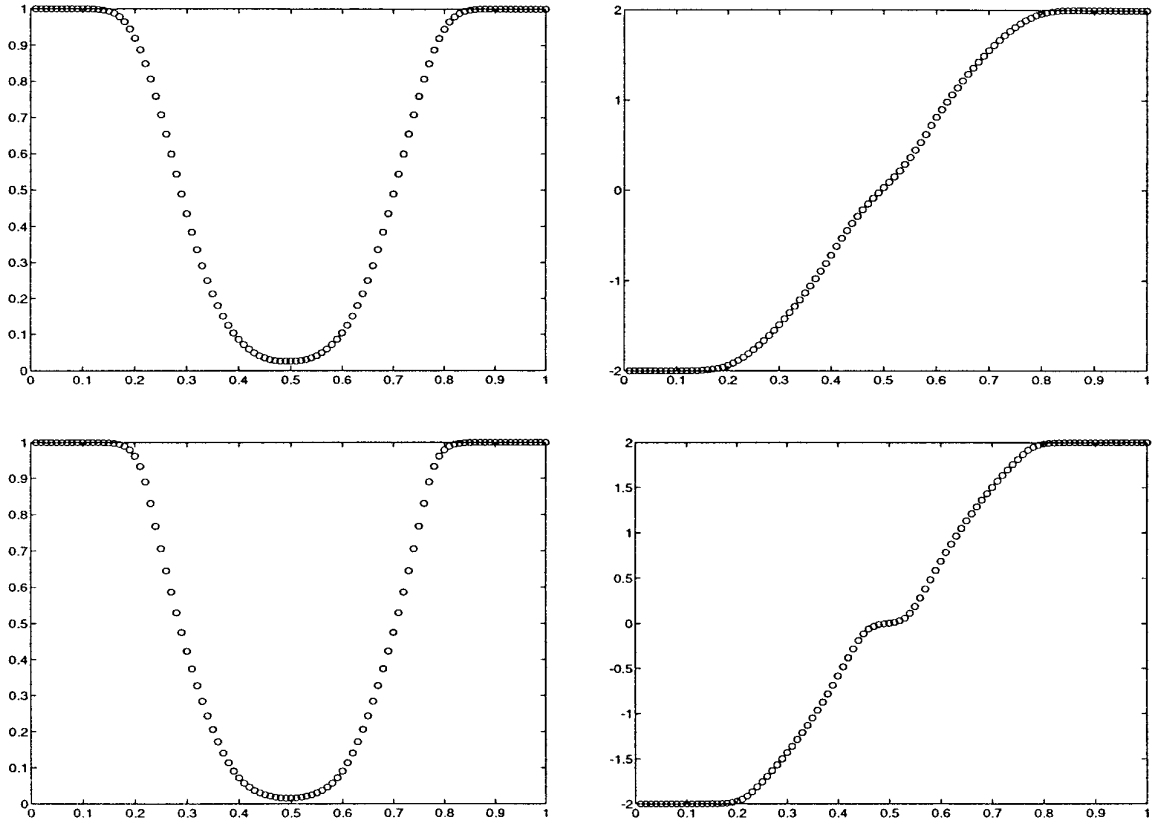

FIG. 7. A non-linearizable Riemann problem. First-order (top) and second-order (ENO-2, bottom) density and velocity profiles (left and right, respectively).

In [1] these authors give a heuristic explanation for the noise generation phenomenon and propose a "cure": the addition of a small amount of artificial dissipation to the underlying scheme.

Roberts [19] performs a deeper analysis of the phenomenon and shows that the cause of the noise generation is linked to the nature of the discrete shock structure produced by a given scheme. Thus, each particular scheme has a different level of this "noise." In fact, it is shown in [18] that the performance of Osher's scheme at a slowly moving shock wave is better than that of Godunov or Roe. Roberts thus concludes by suggesting that numerical flux formulas that recognize the analytical shock jump conditions (such as Godunov's, or Roe's) might be less appropriate for shock capturing than other formulas that do not explicitly recognize those jumps.

In the process of revising this paper for final publication, Osher drew our attention to related work by Jin and Liu [11] on the noise generation at slowly moving shock waves. In Jin and Liu's work, the oscillations are identified as the effect of *diffusion waves,* associated to a given characteristic family, whose influence is non-negligible when the shock speed is small.

Roberts [19] observes, as do Jin and Liu [11], that the noise cannot be eliminated by appealing to TVD concepts. In fact, higher order versions of Godunov's or Roe's scheme accentuate the problem; the noise is preserved for an even longer distance than in the first-order solution.

Quirk [17] reports similar low frequency, postshock oscillations in slowly moving shock waves computed with Einfeld's HLLE scheme [3].

We shall consider the Riemann problem for the Euler equations for an ideal gas ($\gamma = 1.4$) with left and right states given by (Quirk [17]):

$$\begin{aligned}(\rho_l = 3.86, q_l = -0.81, p_l = 10.33)\\ (\rho_r = 1, q_r = -3.44, p_r = 1).\end{aligned} \tag{19}$$

Our numerical solutions are shown after 4000 iterations, after which the shock has crossed about 42 cells.

We can observe in Fig. 9 that the noise generation and transport phenomenon is less acute in Marquina's scheme. It is reasonable to think that the heat conduction mechanism is responsible for the additional dissipation that damps out the downstream noise to computationally acceptable levels.

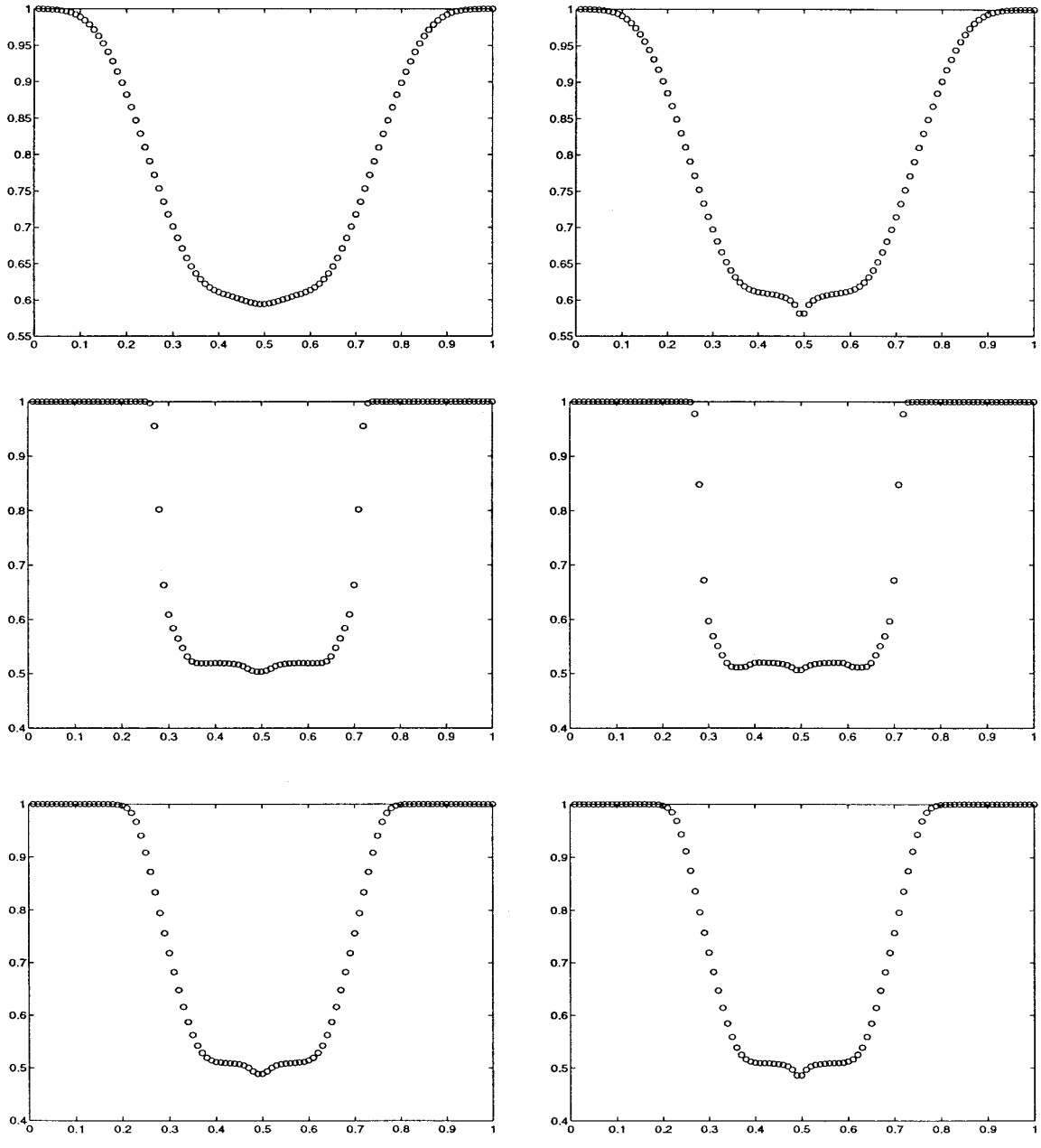

FIG. 8. Non-smooth density behavior in the separation of two rarefaction waves. First-order (top) and third-order (PHM middle and ENO-3 bottom) density profiles; Marquina left, Roe right.

As observed by Roberts [19], the noise is preserved further downstream in higher order extensions of Roe's scheme. On the other hand, the PHM in Marquina's scheme leads to a higher order method with, essentially, the same properties, with respect to the noise phenomenon, as the first-order approximation (see Fig. 10).

6. A TWO-DIMENSIONAL TEST

In this section we consider a two-dimensional test problem introduced by Emery [5] almost 30 years ago, but that has proven to be a useful test for a large number of methods over the years.

The problem begins with a uniform Mach 3 flow in a tunnel containing a step. The tunnel is 3 units long and 1 unit wide. The step is 0.2 units high and is located 0.6 units from the left-hand end of the tunnel. An inflow boundary condition is applied at the left end of the computational domain and outflow boundary conditions are applied at the right end. Along the walls of the tunnel we apply reflecting boundary conditions.

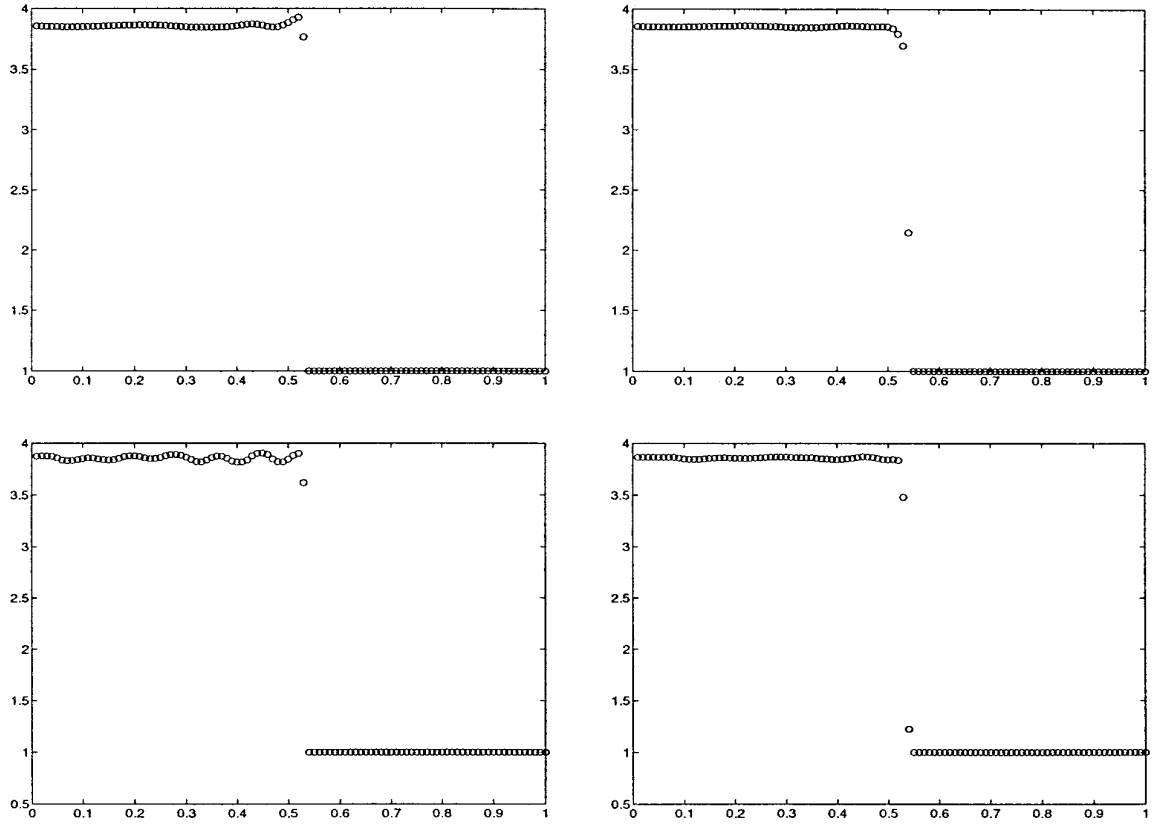

FIG. 9. A slowly moving shock wave: first-order (top) and third-order (PHM, bottom) density profiles: Marquina right, Roe left.

Initially, the wind tunnel is filled with a gamma-law gas, with $\gamma = 1.4$, which everywhere has density 1.4, pressure 1.0, and velocity 3. Gas with this density, pressure, and velocity is continually fed in from the left-hand boundary.

This test problem receives detailed attention in [28], where the authors analyze the behavior of various shock capturing schemes applied to it. We refer the interested reader to this paper (and references therein) for further details and comparisons.

The density distribution is the hardest to compute due, on one hand, to the Mach stem at the upper wall and the contact discontinuity it generates and, on the other hand, to the corner of the step, which is a singularity

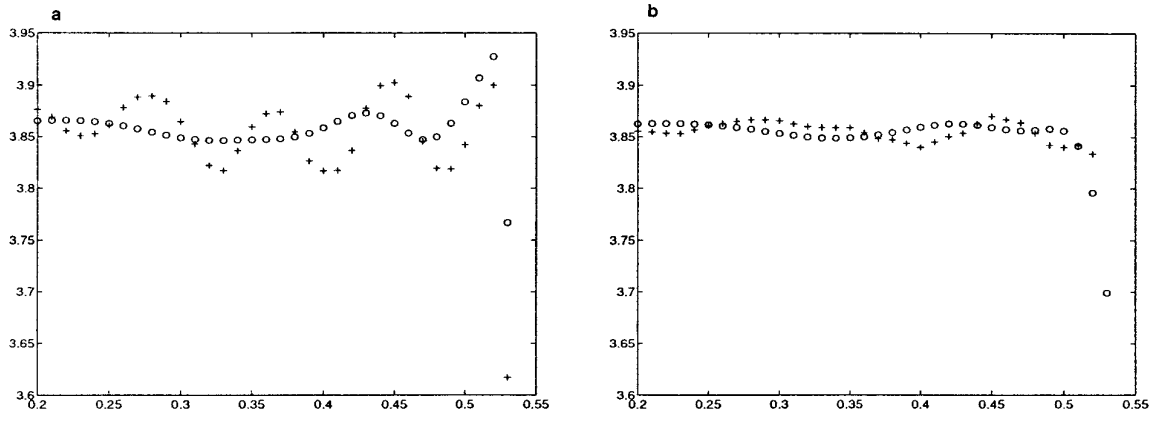

FIG. 10. A closer look at the noise in a slowly moving shock.

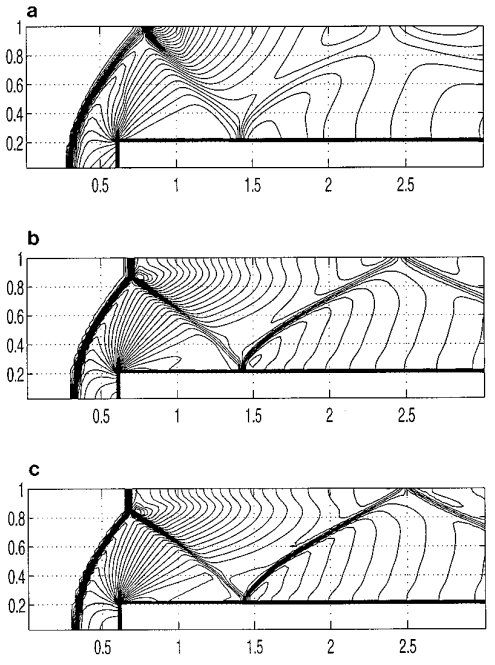

FIG. 11. Contour plots of numerical approximations to the density obtained with Marquina's scheme. First order (a), MUSCL (b), PHM (c).

of the boundary of the domain and the center of a rarefaction fan, i.e., a singular point of the flow.

Woodward and Colella [28] realize that numerical errors generated in the neighborhood of this singular point can seriously affect the global flow. As pointed out in [28], when an approximate Riemann solver is used, the entropy tends to grow near the corner and along the sonic line starting at the corner. If nothing is done, a numerical boundary layer in density, of about one to two zones, builds up and the magnitude of the two components of the velocity decreases along the top of the step, hence changing the quality of the flow.

In an attempt to minimize numerical errors generated at the corner of the step, Woodward and Colella propose an additional boundary condition to be applied near the corner of the step, in order to maintain a steady flow around this singular point. Our experimentation confirms Woodward and Colella's remarks. A detailed treatment of the corner correction is given in the Appendix.

Our numerical tests are run on an equally spaced grid with $h_x = h_y = 1/40$ and we show numerical approximations to the density profile at time $t = 4$, when the flow has a rich and interesting structure. The extension to two dimensions is done by the usual dimensional splitting technique.

Each plot in Figs. 11 and 12 displays 30 equally spaced level curves between the minimum and maximum values of the computed density. Figure 11 shows numerical approximations obtained with Marquina's scheme and Fig. 12 shows those obtained with Roe's scheme

By time $t = 4$, nearly all the shocks in this problem are moving very slowly. In particular, the bow shock is nearly aligned with the grid near the bottom wall, leading to a scenario like the one described in Section 5. The postshock oscillations are more visible when using Van Leer's piecewise linear reconstruction [24].

The Mach stem in Roe's approximation appears severely distorted by a "double kink." This phenomenon is not dissimilar to the "carbuncle," a recognized deficiency of Roe's scheme observed in steady-state blunt body calculations [18].

To eliminate the "carbuncle" produced in Roe's scheme one has to artificially add dissipation to the scheme. Peery and Imlay [18] do so by an appropriate smoothing of the eigenvalues of the Roe matrix. Quirk [17] reports that applying Harten's entropy fix to the contact and shear waves also fixes the problem. Both alternatives become a convenient way to introduce a small (but sufficient) amount of artificial dissipation into the scheme.

As in our one-dimensional tests, Marquina's scheme seems to introduce the right amount of dissipation to eliminate the undesired pathologies, while keeping, at the same time, sharp shock structures.

For the sake of comparison, Fig. 13 shows first and third (PHM) numerical approximations obtained with our two-dimensional version of the flux vector splitting

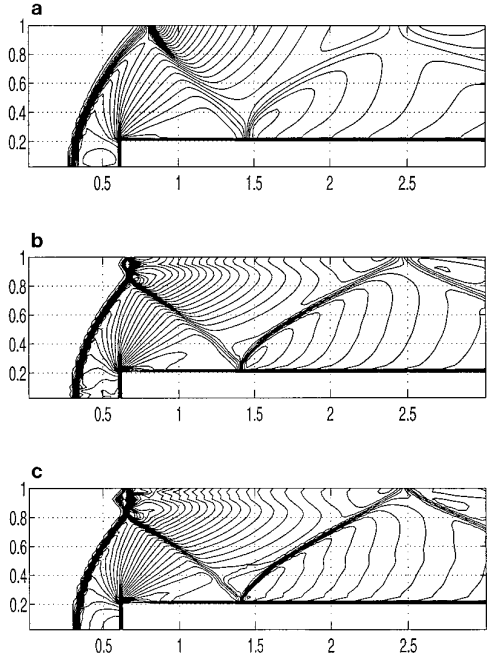

FIG. 12. Contour plots of numerical approximations to the density obtained with Roe's scheme.

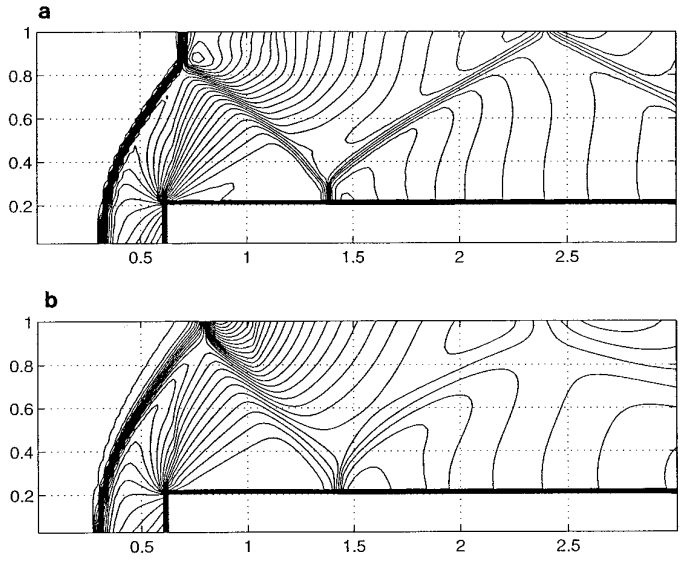

FIG. 13. Contour plots of numerical approximations to the density obtained with Steger and Warming's scheme.

scheme of Steger and Warming. The behavior of the first-order scheme (for this resolution) is similar to the one obtained with Marquina's and Roe's schemes; however, there are no traces of the contact discontinuity emerging from the three-shock interaction in the third-order approximation. Also, Marquina's scheme seems to lead to a smoother behavior in the rarefaction fan in this case.

7. CONCLUSIONS

We extend to the systems a numerical flux formula proposed by Shu and Osher [22] for scalar equations. The extension is made in each local characteristic field and does not need a mean state (such as Roe's average or the arithmetic mean) which turns out to be useful in certain situations, where even an approximate solution to the Riemann problem is difficult to compute.

Marquina's flux formula seems to introduce a dissipative mechanism into the numerical scheme which, in turn, produces numerical approximations with a smoother behavior than those obtained with Roe's scheme, while keeping, essentially, the sharp shock resolution of this method. In particular, the overheating phenomenon observed near the piston wall in shock reflection experiments is greatly reduced, as well as the long wavelength noise behind slowly moving shock waves.

Preliminary experimentation in two dimensions seems to indicate that the dissipation of the scheme is sufficient to eliminate undesired pathologies like the carbuncle phenomenon.

APPENDIX: DISCUSSION OF THE CORNER TREATMENT

In order to go further into the discussion of the influence of the corner treatment in Emery's test, we shall explain in detail the process introduced in [28] and outlined in [21] (where we have observed various typographical errors).

We shall perform two successive corrections on certain cells, which we call "b," above the step; using the values of the variables at the cell located just to the left and below the corner, we call this cell "a" (as in [21]). The "b" cells are the first four cells of the first row above the step starting just to the right of the corner, and the first two cells of the second row above, also starting from the right.

The corrections should be as follows:

• *Entropy correction.* In each "b" cell, we reset the density in order for the adiabatic constant in cell "b," to be the same as in cell "a,"

$$\rho_{\mathrm{b}} = \rho_{\mathrm{a}} \left(\frac{P_{\mathrm{b}}}{P_{\mathrm{a}}} \right)^{1/\gamma}. \tag{20}$$

• *Enthalpy correction.* Using the reset density value, we correct the enthalpy in "b" cells, by changing the magnitudes of the velocities (not their directions!) as follows:

There is always a nonnegative constant α such that

$$H_{\mathrm{a}} = H_{\mathrm{b}}^{\alpha}, \tag{21}$$

where H_{a} is the enthalpy in cell "a," and

$$H_{\mathrm{b}}^{\alpha} = \frac{c_{\mathrm{b}}^2}{(\gamma - 1)} + \frac{1}{2} \alpha q_{\mathrm{b}}^2 \tag{22}$$

with q_{b}^2 being the sum of the squares of the original components of the velocity in cell "b," and c_{b} being the sound velocity computed from the new value of the density also in cell "b." Equation (21) is just *Bernouilli's law* for steady flow (see [2]), and it always has a nonnegative solution for α, because the value of the density in "b" cells is never larger than the value in cell "a."

Indeed, if $A = P_{\mathrm{a}}/\rho_a^{\gamma}$ is the adiabatic constant in cell "a," then, because of the entropy correction performed before, we have that $A = P_{\mathrm{b}}/\rho_{\mathrm{b}}^{\gamma}$, and, therefore, α is nonnegative and defined by

$$\alpha = \left[\frac{1}{2} q_a^2 + \frac{\gamma}{\gamma - 1} A (\rho_a^{\gamma - 1} - \rho_{\mathrm{b}}^{\gamma - 1}) \right] \Big/ \frac{1}{2} q_{\mathrm{b}}^2 . \tag{23}$$

We then reset the vector $\mathbf{u}$ in each "b" cell to

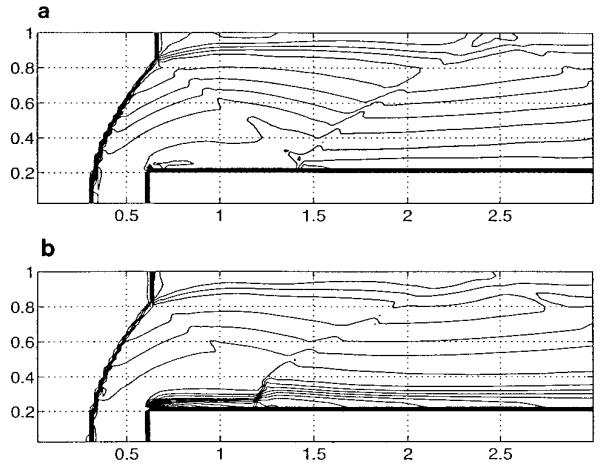

FIG. 14. Contour plots of the adiabatic constant P/ρ^{γ}. Notice the entropy violation at the corner of the step without the corner treatment (bottom).

$$\left(\rho_{\mathrm{b}}, \sqrt{\alpha}(q_{\mathrm{b}})_x, \sqrt{\alpha}(q_{\mathrm{b}})_y, \frac{1}{\gamma-1}\rho_{\mathrm{b}} + \frac{1}{2}\rho_{\mathrm{b}}\alpha q_{\mathrm{b}}^2\right). \quad (24)$$

If these two successive corrections are not applied the adiabatic constant (and *a fortiori* the entropy) is violated along the streamlines just above the step.

In Fig. 14 we display two contour plots of the adiabatic constant at $t = 4$. They correspond to numerical approximations obtained with Marquina's scheme and the PHM as the reconstruction procedure. Figure 14a corresponds to the application of the corner treatment and 14b is without this treatment.

We have observed that, when no treatment is applied, the value of the enthalpy above and near the corner is slightly smaller than the value at the left of the corner. Thus the fluid there is almost steady; however, the entropy is clearly violated and we get pictures analogous to the ones presented in [27].

The reason we need to apply the two corrections is that if only the entropy is corrected then the flow near the corner becomes far from steady, and the enthalpy is abruptly going down at the right of the sonic line (see Fig. 15).

The section $y = 0.2$ of the adiabatic constant is shown in Fig. 15 for both cases. We observe a strong entropy violation at $x = 0.6$, the abscissa of the corner. This section can be considered nearly a streamline of the flow.

We consider this a fair numerical test in order to evaluate the reliability of the numerical approximation. We have computed numerical approximations to the solution of this problem using our solver with a finer grid (e.g., 240×80), and the profiles obtained are consistent with the features presented with the 120×40 grid and the order of accuracy used.

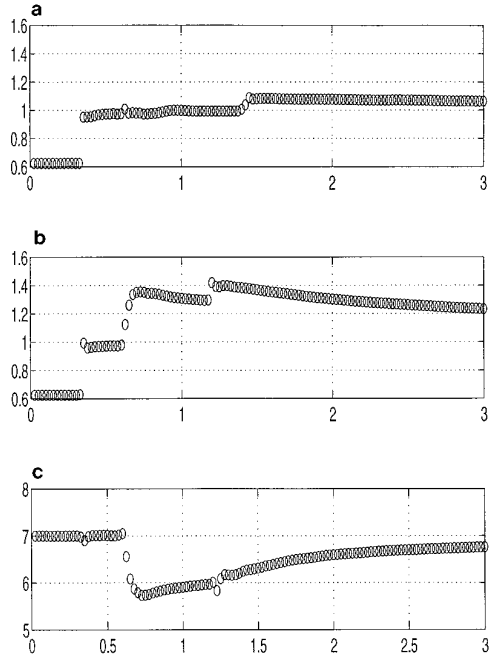

FIG. 15. One-dimensional section cuts, at the corner of the step, for the adiabatic constant and the enthalpy.

ACKNOWLEDGMENTS

The authors thank J. M. Ibañez, J. M. Marti, and J. A. Font for many useful discussions and comments. We also thank S. Osher, A. Harten, and R. Menikoff for their valuable remarks and suggestions. We especially thank P. L. Roe and the referees of this paper for their remarks and for providing several useful references.

REFERENCES

1. P. Colella and P. R. Woodward, *J. Comput. Phys.* **54,** 174 (1984).
2. R. Courant and K. O. Friedrichs, *Supersonic Flow and Shock Waves* (Springer-Verlag, New York 1976).
3. B. Einfeldt, *SINUM* **25,** 294 (1988).
4. B. Einfeldt, C. D. Munz, P. L. Roe, B. Sjögreen, *J. Comput. Phys.* **92,** 273 (1991).
5. A. F. Emery, *J. Comput. Phys.* **2,** 306 (1968).
6. P. Glaister, *J. Comput. Phys.* **74,** 382 (1988).
7. A. Harten and J. M. Hyman, *J. Comput. Phys.* **50,** 235 (1983).
8. A. Harten, J. M. Hyman, and P. D. Lax, *Commun. Pure Appl. Math.* **29,** 297 (1976).
9. A. Harten, P. D. Lax, and B. van Leer, *SIAM Rev.* **25,** 35 (1983).
10. A. Harten, B. Engquist, S. Osher, and S. Chakravarthy, *J. Comput. Phys.* **71**(2), 231 (1987).
11. S. Jin and J. G. Liu, reprint.
12. R. J. Leveque, *Numerical methods for Conservation Laws* (Birkhauser, Zurich, 1990).
13. A. Marquina, UCLA CAM Report No. 25-(1989); *SIAM J. Sci. Comput.* **15,** 892 (1994).
14. R. Menikoff, *SIAM J. Sci. Comput.* **15,** 1242 (1994).
15. W. F. Noh, *J. Comput. Phys.* **72,** 78 (1987).

16. S. Osher and F. Solomon, *Math. Comput.* **38,** 339 (1982).
17. J. Quirk, *Int. J. Numer. Methods Fluids* **18,** 555 (1994); ICASE Rep. 92-64, 1992.
18. K. M. Peery and S. T. Imlay, AAIA Paper 88-2904 (unpublished).
19. T. W. Roberts, *J. Comput. Phys.* **90,** 141 (1990).
20. P. L. Roe, *SIAM J. Sci. Comput.* **13**(2), 611 (1992).
21. R. Sanders and A. Weiser, *J. Comput. Phys.* **101,** 314 (1992).
22. C. W. Shu and S. J. Osher, *J. Comput. Phys.* **83,** 32 (1989).
23. J. Steger and R. F. Warming, *J. Comput. Phys.* **40,** 263 (1981).
24. B. Van Leer, *J. Comput Phys.* **32,** 101 (1979).
25. B. Van Leer, *SIAM J. Sci. Stat. Comput.* **5,** 1 (1984).
26. B. Van Leer, ''Flux-Vector Splitting for the Euler Equations,'' in *8th International Conference on Numerical Methods for Engineering, Aachen, June 1982.*
27. P. R. Woodward and P. Colella, ''High Resolution Difference Scheme for Compressible Gas Dynamics,'' in *''Seventh International Conf. on Numer. Methods in Fluid Dynamics,* Lecture Notes in Physics, Vol. 141, pp. 434-441, (Springer-Verlag, New York/Berlin, 1981).
28. P. R. Woodward and P. Colella, *J. Comput. Phys.* **54,** 115 (1984).